

Bioinspiration for Anisotropic Load Transfer at Soil–Structure Interfaces

Alejandro Martinez, Ph.D., A.M.ASCE¹; Sophia Palumbo²;
and Brian D. Todd, Ph.D.³

Abstract: Load transfer across soil–structure interfaces plays an important role in the capacity and efficiency of many geotechnical applications. Some geotechnical applications may benefit from soil–structure interfaces that mobilize different amounts of shear resistances depending on the direction of loading. Bioinspiration is used in this study to develop a series of surfaces modeled after the ventral scales of different snake species that exhibit anisotropic interface shear behavior. The frictional behavior of the snakeskin-inspired surfaces was assessed by means of interface shear box tests on sand specimens composed of two different sands. The results indicate a prevalent anisotropic behavior, where shearing in the cranial direction (i.e., against the scales) mobilized larger peak and residual interface strength and dilation than shearing in the caudal direction (i.e., along the scales). A parametric study on the geometrical characteristics of the scales revealed the isolated effect of their height and length, and particle image velocimetry analyses revealed larger soil deformations and dilation induced within the soil during cranial shearing. The scale geometry ratio is shown to qualitatively capture the interface load-transfer mechanisms between the sand and different bioinspired surfaces. DOI: [10.1061/\(ASCE\)GT.1943-5606.0002138](https://doi.org/10.1061/(ASCE)GT.1943-5606.0002138). © 2019 American Society of Civil Engineers.

Introduction

Load transfer across soil–structure interfaces plays an important role in the capacity and efficiency of many geotechnical engineering applications. In some cases, mobilization of large shear resistances is desired because this translates to increases in load-carrying capacity, such as for axially loaded deep foundations, soil nails, tiebacks, geogrids, and geomembranes. In other cases, minimization of shear resistances is desired, such as during pile driving, tunneling, and soil sampling. Some applications can benefit from soil–structure interfaces that mobilize different amounts of shear resistances depending on the direction of loading, referred throughout this paper as frictional anisotropy. With such a soil–structure interface, a soil anchor, for example, would mobilize smaller resistances during installation than during subsequent tensile loading.

Bioinspiration for frictional anisotropy can be obtained from different biological adaptations, such as the paws of certain mammals and birds, the leaves of some trees and grasses, and the skin of several reptiles. Without limbs, snakes are efficiently mobile in a variety of environments, from sand dunes to trees, forest litter, prairies, and oceans. Snakes can burrow in soil, climb steep slopes and trees, move through loose granular material, and swim (Marvi et al. 2014). Their ventral scales are oriented transversely along their underbody (Fig. 1), and their frictional interactions with the

substrate control the snake's locomotive abilities. Studies of snake ventral scale morphology and tribology have shown that they exhibit frictional anisotropy when displaced in the forward (caudal), backward (cranial), and lateral directions (Benz et al. 2012). For instance, Gray and Lissmann (1950) measured the coefficient of friction, μ , between sandpaper and dead snakes transported cranially and caudally. They measured a larger μ (1.22) in the cranial direction than in the caudal direction (0.49).

Marvi and Hu (2012) and Marvi (2013) measured μ for three live snakes in contact with a rough Styrofoam polystyrene foam substrate. The ventral scales of three species mobilized a μ that was between 40% and 300% greater in the cranial than in the caudal direction. Marvi et al. (2016) investigated the ability of snakes to control the angle of attack of their scales during locomotion. The authors provided evidence indicating that indeed the snakes change their scale angle of attack using muscles underneath their belly skin. This mechanism allows them to actively influence the friction generated between their skin and the substrate. Snakeskin also has a hierarchical structure with nanoscale features called denticles within each scale. The denticles have a highly asymmetric geometry that allows for interlocking with nanoscale surface features and particles. These interactions further allow the snakes to mobilize a smaller amount of friction during forward scale movement, relative to the substrate, than during backward scale movement (Hazel et al. 1999).

Bioinspiration typically is used in engineering to complement or enhance existing solutions. Thus, the results presented in this paper build on previous advancements in the understanding of interface shear behavior, including the effect of surface roughness magnitude and form, particle angularity and size, soil density, soil fabric, gradation, particle breakage, surface damage and wear, loading conditions, and boundary conditions (e.g., Uesugi and Kishida 1986; Uesugi et al. 1989; Hryciw and Irsyam 1993; Subba Rao et al. 1998; Dove and Frost 1999; Dove and Jarrett 2002; Dietz and Lings 2006; DeJong and Westgate 2009; Ho et al. 2011; Vangla and Latha 2015; Martinez et al. 2015; Martinez and Frost 2017; Farhadi and Lashkari 2017).

¹Assistant Professor, Dept. of Civil and Environmental Engineering, Univ. of California, Davis, CA 95616 (corresponding author). ORCID: <https://orcid.org/0000-0003-4649-925X>. Email: amart@ucdavis.edu

²Staff Engineer, Geosyntec Consultants, 1111 Broadway St., 6th floor, Oakland, CA 94607. ORCID: <https://orcid.org/0000-0003-2444-4370>. Email: spalumbo@geosyntec.com

³Associate Professor, Dept. of Wildlife, Fish, and Conservation Biology Univ. of California, Davis, CA 95616. Email: btodd@ucdavis.edu

Note. This manuscript was submitted on September 27, 2018; approved on May 2, 2019; published online on July 27, 2019. Discussion period open until December 27, 2019; separate discussions must be submitted for individual papers. This paper is part of the *Journal of Geotechnical and Geoenvironmental Engineering*, © ASCE, ISSN 1090-0241.

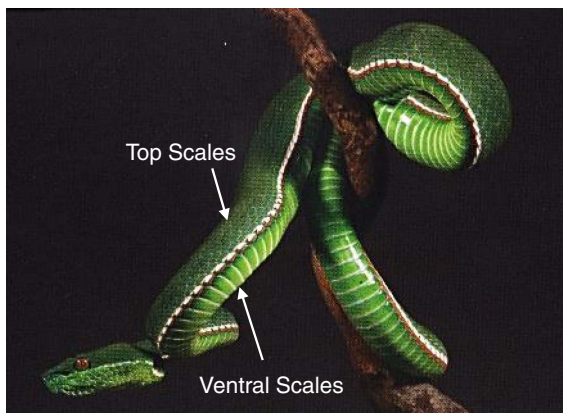


Fig. 1. Tree snake showing ventral (belly) and dorsal (top) scales. (Adapted from H. B. Lillywhite, *How Snakes Work: Structure, Function and Behavior of the World's Snakes*, © 2014, with permission of Oxford Publishing Ltd. through PLSclear.)

Bioinspiration

Selection of Biological Mechanisms

In research and engineering design, the bioinspiration process, consisting of distilling, abstracting, and idealizing particular biological adaptations, is commonly iterative. The problem-driven approach consists of the study of nature to obtain a solution for a specific engineering problem. This requires the engineer to have access to the proper knowledge in biology to identify appropriate solutions. On the other hand, the solution-driven approach consists of the search for an engineering application to which an existing natural solution can be applied (Zhou 2000; Helms et al. 2009). In both approaches, a bioinspired solution can be a form, behavior, or principle (Mak and Shu 2004; DeJong et al. 2017). Part of the bioinspiration procedure consists of addressing differences in constraints, spatial and temporal scales, and boundary conditions between the biological and engineering domains (Goel et al. 2014; Frost et al. 2017).

The abstracted engineering problem in this research is the need to mobilize frictional anisotropy at soil–structure interfaces. Fig. 2 presents three different mechanisms that snakes use to cope with this engineering problem. As a surface in contact with the skin slides against the sharp scale edges (i.e., in the cranial direction),

the frictional resistances are relatively large due to three distinct mechanisms: (1) the scales' asymmetric profile that allows them to latch on asperities, (2) scale compliance that results in scale deformation, such that the contact area with the sliding surface is increased, and (3) control of the scale angle of attack that also increases contact area. Conversely, as a surface slides along the scales (i.e., in the caudal direction), the mobilized frictional resistances are smaller due to (1) the inability of scales to latch on asperities, (2) scale compliance leading to a reduction in contact area, and (3) control of angle of attack that also decreases the contact area. The adaptation used in this research is the asymmetric shape of the scales, such that the shear resistances mobilized by soil–structure interfaces sheared in the cranial direction are expected to be larger than those mobilized in the caudal direction.

Translation of biological solutions to the engineering domain requires evaluation of the boundary conditions in both the biological and engineering realms. One important difference between the conditions imposed on a snake and on a geotechnical system deployed in the field is the magnitude of effective stresses: a snake typically experiences effective stresses smaller than 10 kPa, whereas a geotechnical system can be subjected to effective stresses on the order of hundreds to thousands of kilopascals. It is currently unclear whether the geometry of typical snakeskin will produce frictional anisotropy under larger levels of effective stress. For this reason, instead of directly mimicking the skin geometry of specific snake species, the focus of this investigation is to explore the influence of profile geometry on the mobilized interface shear behavior.

Generation of Bioinspired Surface Profiles

A total of 60 preserved snake specimens were borrowed from the Museum of Vertebrate Zoology at the University of California, Berkeley. Approximately 30 different species were obtained such that two specimens represented almost every species. The species encompassed snakes that habituate in diverse environments, perform different locomotive behaviors, and interact with various types of substrates. The mass, average diameter, and head-to-tail length of each snake was recorded. Two ventral skin scans were performed on each snake specimen using a white-light scanner with a resolution of $0.1 \mu\text{m}$ (VR-3100, Keyence, Osaka, Japan). Scan locations were constrained to the midlength portion of the snake body. A surface shape correction was applied to the scans, and two horizontal profiles were obtained from each scan, for a total of four ventral skin profiles per snake.

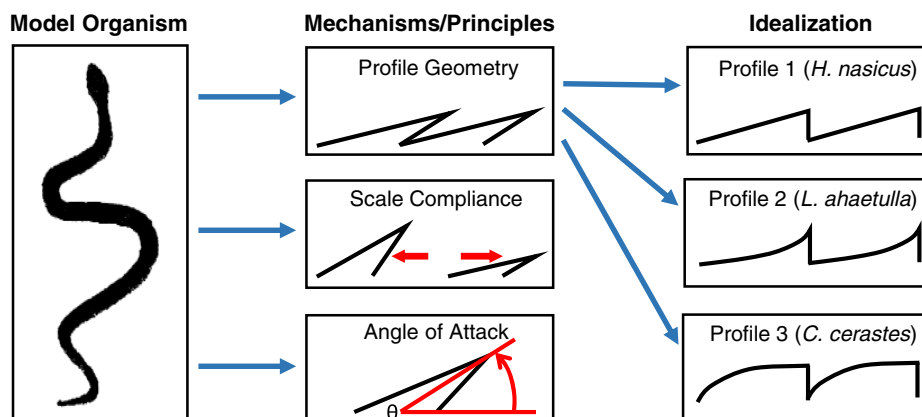


Fig. 2. Flowchart of bioinspiration process.

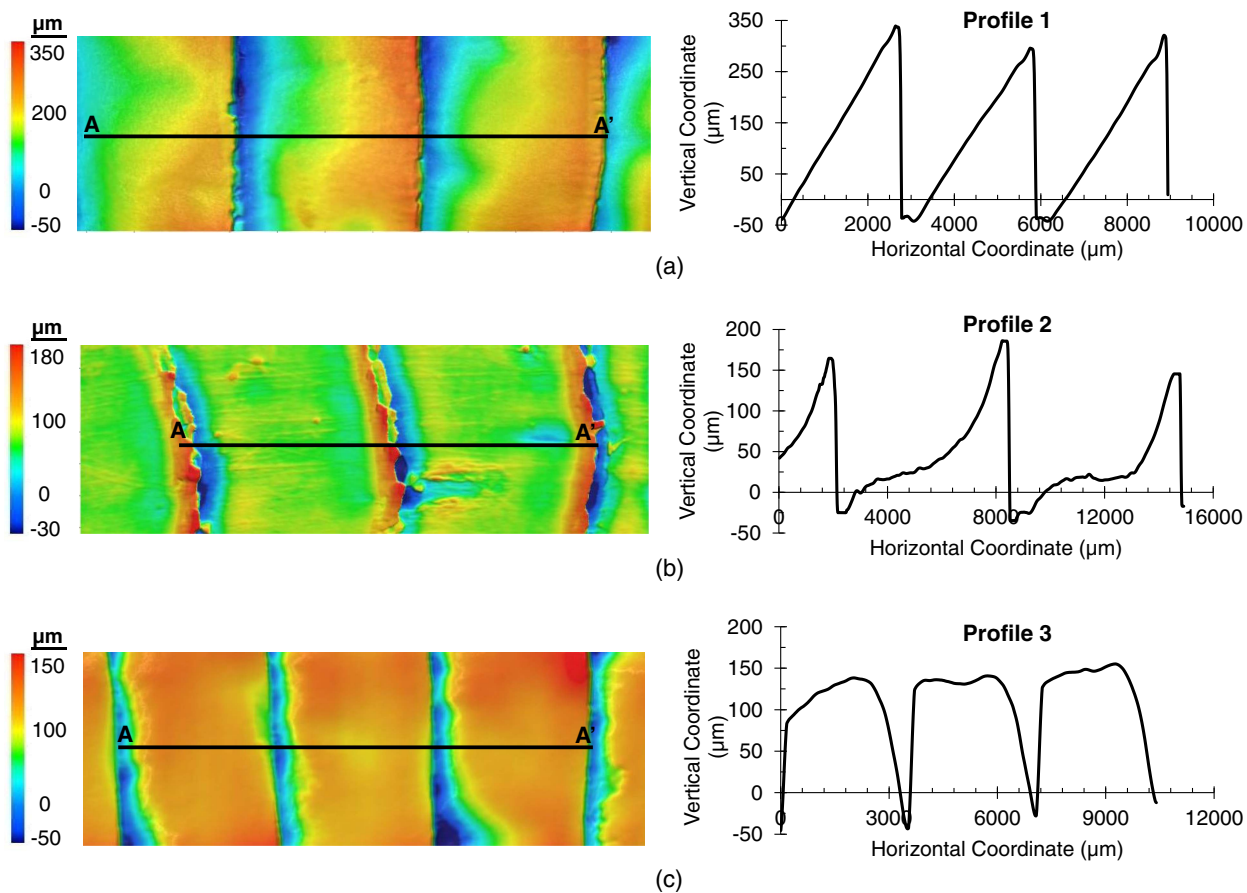


Fig. 3. Three-dimensional scans and profiles of skin of (a) *Heterodon nasicus*; (b) *Leptophis ahaetulla*; and (c) *Cerastes cerastes*.

Table 1. Characteristics of profiles for snakeskin-inspired surfaces

Profile type	Species	Common name	Environment	Characteristic behavior
1	<i>Heterodon nasicus</i>	Western hognose snake	Prairie and forest floor	Litter dwelling
2	<i>Leptophis ahaetulla</i>	Parrot snake	Arboreal	Tree climbing
3	<i>Cerastes cerastes</i>	Saharan horned viper	Desert	Sidewinding

Ventral scale profiles were evaluated to identify patterns in surface roughness form. Three profile types representing the most commonly occurring profiles in the scans were chosen as models for the bioinspired surfaces. Ventral scale scans and surface profiles of the snakes considered in this study are presented in Figs. 3(a–c). The first ventral scale profile, Profile 1, was of a Western hognose snake (*Heterodon nasicus*), which has a straight-lined, triangular scale shape [Fig. 3(a)]. *H. nasicus* is a prairie- and generally litter-dwelling-snake that engages in various modes of locomotion such as burrowing (Durso 2011). Profile 2 is of a tree-climbing parrot snake (*Leptophis ahaetulla*), which has concave-shaped scales to enhance its grip during climbing [Fig. 3(b)]. Profile 3 is of a Saharan horned viper (*Cerastes cerastes*), a desert dwelling sidewinder with convex-shaped scales [Fig. 3(c)] that assist the snake when propelling off of loose granular soils (Marvi et al. 2014). The geometry of the three profile types was idealized (Fig. 2) and extruded onto a planar surface to allow for manufacture of the surfaces using three-dimensional additive manufacturing. Table 1 presents a summary of the characteristics of each profile type.

Experimental Methods and Materials

Bioinspired Surfaces

A total of 19 bioinspired surfaces were tested as part of this research. All surfaces were 3D printed with the Form 2 printer (Formlabs, Sommerville, Massachusetts), which uses stereolithography (SLA) technology to create objects made of methacrylate photopolymer liquid resin. The printer applies a laser to selectively cure and solidify the resin. The specific gravity of the solid resin is 1.18, its Young's modulus is 3.6 GPa, its ultimate tensile strength is 71.5 MPa, and its Rockwell hardness is 45.7 (Palumbo 2018). All surfaces were manufactured using a 3D-printed lift thickness of 50 μm . Preliminary tests deemed the resin suitable for testing in the shear box without sustaining significant wear at normal effective stresses smaller than or equal to 150 kPa (Martinez and Palumbo 2018).

The height and length of the surface asperities, herein referred to as scales, were parametrically varied. The scale height, H , ranged from 0.10 to 0.72 mm, and the scale length, L , ranged from 6 to

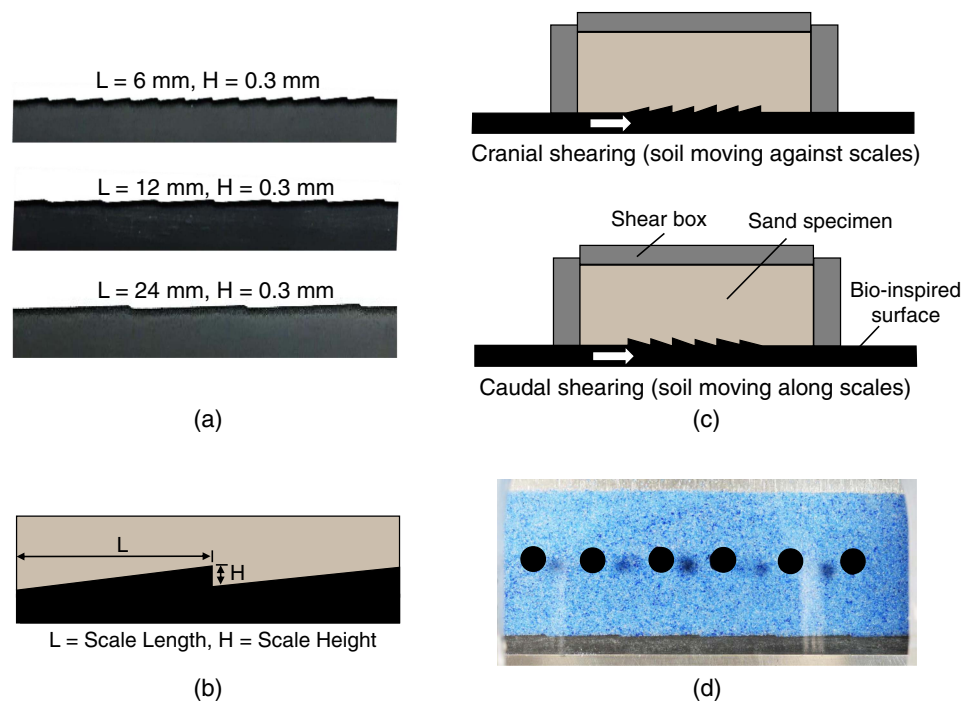


Fig. 4. (a) Photographs of 3D-printed bioinspired surfaces; (b) schematic of scale geometrical characteristics; (c) cranial and caudal testing configurations; and (d) photograph of dyed sand specimen for PIV analysis.

32 mm [Figs. 4(a and b) and Table 2]. Tests against surfaces of varying H and L were performed to study the effect of scale geometry on the interface strength and frictional anisotropy. During an interface shear test, the surface was displaced either in the cranial (against the scales, toward the snake's head) or in the caudal (along the scales, toward the snake's tail) directions, as shown in Fig. 4(c). The central portion of the surfaces was textured with the bioinspired design over a length of 80 mm. Untextured areas with a length of about 11 mm were manufactured on either side of the textured

section to minimize boundary effects, as done by other authors (e.g., DeJong et al. 2003; Martinez and Stutz 2019). Two additional surface types, epoxied Ottawa 20-30 sand on steel (referred to as glued sand, with an average surface roughness, R_a , of $133 \mu\text{m}$), and untextured resin (referred to as untextured surface, with R_a of $7 \mu\text{m}$) were tested in this study. Tests against these two surfaces provided data for comparison with the cases of a fully rough and smooth interfaces. A detailed description of the surfaces tested has been provided by Palumbo (2018).

Table 2. Geometrical parameters of snakeskin-inspired surfaces

Profile type	Scale height, H (mm)	Scale length, L (mm)	Scale geometry ratio, L/H	Average surface roughness, R_a (mm)	Test on F-65	Test on O20-30
1	0.10	12	120.0	0.027	X	—
	0.10	18	180.0	0.023	X	X
	0.10	24	240.0	0.016	X	X
	0.15	12	80.0	0.039	X	X
	0.15	24	160.0	0.035	X	X
	0.30	6	20.0	0.086	X	X
	0.30	12	40.0	0.081	X	X
	0.30	18	60.0	0.082	X	X
	0.30	24	80.0	0.081	X	X
	0.30	32	106.7	0.071	X	X
2	0.72	12	16.7	0.196	X	X
	0.30	6	20.0	0.069	—	X
	0.30	12	40.0	0.078	—	X
	0.30	18	60.0	0.076	—	X
3	0.72	12	16.7	0.134	—	X
	0.30	6	20.0	0.079	X	X
	0.30	12	40.0	0.068	X	X
	0.30	18	60.0	0.085	X	X
Glued sand	—	—	—	0.133	X	X
	—	—	—	0.007	X	X

Table 3. Grain size, packing, and strength properties of tested sands

Parameter	Ottawa F-65	Ottawa 20-30
G_s	2.65	2.65
D_{50} (mm)	0.20	0.72
C_u	1.61	1.17
C_c	0.96	0.96
e_{\max}	0.83	0.72
e_{\min}	0.51	0.54
φ_{peak} (degrees) ^a	33.8	38.5
$\varphi_{\text{residual}}$ (degrees) ^a	29.6	29.2

^aDirect shear using a 6.35 cm (2.5 in.) shear box.

Sands Tested

Ottawa 20-30 (O20-30) and Ottawa F-65 (F-65) sands were tested in this study to investigate the effect of particle size on the interface shear response of the bioinspired surfaces. Both quartz sands are poorly graded with a subrounded particle shape. O20-30 has a mean particle diameter, D_{50} , of 0.72 mm, and F-65 has a D_{50} of 0.20 mm. Table 3 provides grain size, packing, and strength properties of both sands. All specimens were air-pluviated in the shear box placed over the bioinspired surface to a target relative density of 80%. The specimen length and width were 101.6×63.5 mm, respectively, and the height varied from 22 to 24 mm.

Shear Box Interface Shear Tests

The Geotac Automated Direct Shear System, (Geocomp, Houston, Texas), was modified for direct interface shear testing by fitting a plate to the traveling sled on which the testing surface is fastened, as described by DeJong and Westgate (2009) and Martinez and Stutz (2019). The system includes a vertical actuator that applies a normal load to the specimen, a horizontal actuator that applies a shear force, and an integrated data-acquisition system. The horizontal and vertical displacements were measured with linear potentiometers, and the normal and shear loads applied to the sand specimen were measured using load cells. A reaction arm transferred the friction force generated at the soil–structure interface to the horizontal load cell. Measurements of external box friction indicated a magnitude of about 2 kPa that remained approximately constant for at least 10 mm of shear displacement. Thus, all shear-stress data presented herein was corrected by subtracting 2 kPa from the measured values. The rectangular shear box was composed of three smooth aluminum sides and a smooth borosilicate glass side that allowed for imaging of the soil during testing. The shear stress mobilized at the interface was computed as the measured shear force divided by the specimen cross-sectional area, and the stress ratios were computed as the shear stress divided by the normal stress applied on the specimen. The top cap of the shear box was not restrained to prevent rotation to ensure that the normal stress applied on the specimen remained constant during the entire test. Constant monitoring of the shear box during testing confirmed that a gap between the bioinspired surface and the shear box did not develop during testing.

All the tests were performed under constant normal load (CNL) conditions at a constant normal effective stress of 75 kPa, allowing the specimen to experience vertical deformation in the form of contraction or dilation. During shear testing, the horizontal actuator displaced the surface at a rate of 1 mm/min. Tests on O20-30 sand were performed against surfaces with Profiles 1, 2, and 3; however, tests on F-65 sand were only performed against surfaces with Profiles 1 and 3 (Table 2).

Particle Image Velocimetry

A subset of the tests on F-65 sand was repeated to quantify soil deformations near the interface with particle image velocimetry (PIV). The sand was dyed with blue India ink to enhance its color contrast and improve the results obtained from the PIV analyses [Fig. 4(d)]. Direct shear tests performed on dyed sand specimens indicated that the ink had a no effect on the peak and residual friction angles.

PIV involves analyzing a series of digital photographs to track displacements of image subsets, which are the elements of the mesh that is used to divide the images. The PIV software GeoPIV-RG version 1.0 (Stanier et al. 2016) was utilized for analysis. This software is the updated version of GeoPIV (White et al. 2001), employing a reliability guided computation process for more accurate measurements of small and large soil deformations. GeoPIV-RG also allows for the subsets to deform by using shape functions that describe first-order displacement and displacement gradients, including compression, tension, and shear deformations. Detailed information regarding GeoPIV-RG has been given by Stanier et al. (2016).

The analyses were performed on the portions of the specimens that were visible through the viewing window, constituting their central two-thirds. All the analyses were performed with a correlation coefficient larger than 0.8 and mesh sizes between 50 and 100 pixels, which correspond to 0.75–1.5 mm. All photographs were captured with a Nikon D3200 digital camera (Nikon, Tokyo, Japan) equipped with a Nikon 35-mm f/2D lens, and two light-emitting diode (LED) lights provided adequate lighting. Photographs were captured every 3 s, providing one image every 0.05 mm of surface displacement.

Results

The experimental testing campaign consisted of 66 interface shear tests performed against bioinspired surfaces and four tests performed against the glued sand and untextured surfaces. All results presented herein correspond to monotonic interface shear tests to a target shear displacement of 6 mm where positive vertical displacements indicate specimen dilation.

Interface Shear Behavior of Bioinspired Surfaces

Surfaces with Profile types 1, 2, and 3, presented in Table 2, were tested to investigate the effect of scale shape on the interface shear response. Figs. 5(a and b) present the results from tests on O20-30 specimens sheared against surfaces with Profiles 1, 2, and 3. All profiles had a scale height of 0.3 mm and scale length of 12 mm and were tested in the cranial direction (i.e., against the scales). The surface with Profile 1 mobilized the largest peak and residual shear resistances as well as larger dilative volume changes, followed by the surface with Profile 2 and then by the surface with Profile 3. Figs. 5(c and d) present the results for tests performed with the same surfaces in the caudal direction (i.e., along the scales), indicating larger peak shear resistances and dilative volume changes mobilized by the Profile 1 surface, followed by the Profile 2 and 3 surfaces, respectively.

Shearing in the cranial direction mobilized larger overall shear resistances compared with shearing in the caudal direction. Frictional anisotropy is calculated herein as the difference between the shear resistances (peak or residual) mobilized in the cranial and caudal directions, where positive values indicate larger shear stresses mobilized in the cranial direction. This calculation is performed for test pairs (i.e., cranial and caudal tests performed with

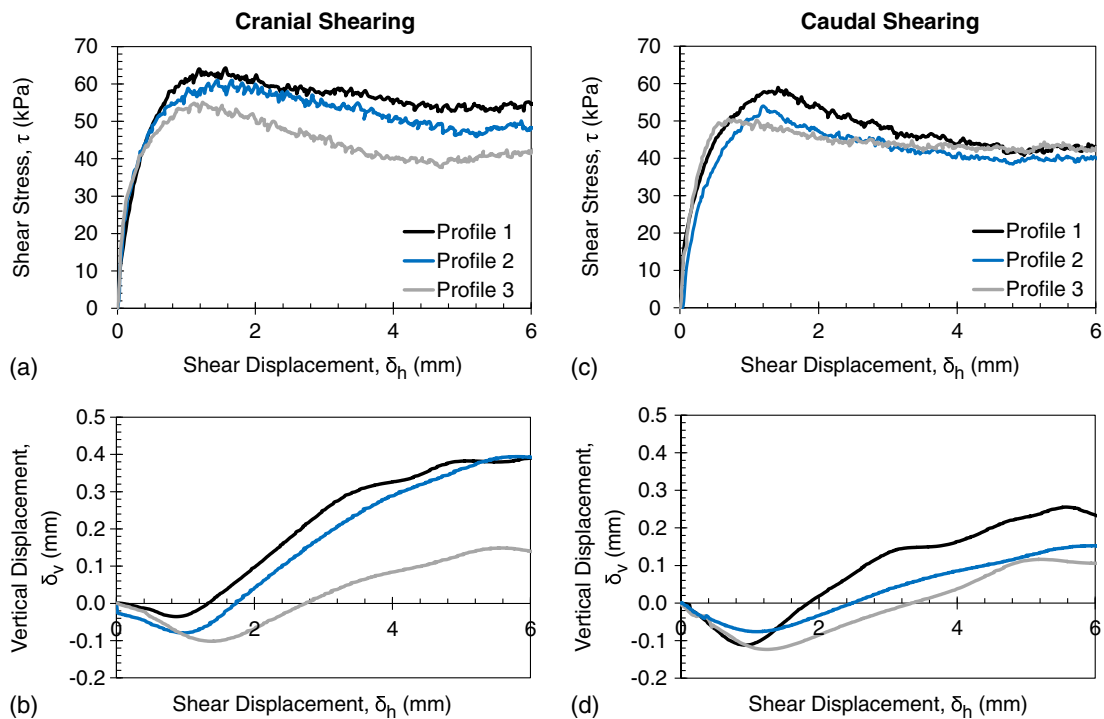


Fig. 5. Mobilized shear stresses and associated vertical displacements for interface shear tests on Ottawa 20-30 sand specimens against surface Profiles 1, 2, and 3 ($H = 0.30$ mm and $L = 12$ mm) in (a and b) cranial; and (c and d) caudal directions.

the same sand against surfaces with the same H and L). Figs. 6(a and b) present average anisotropy values obtained from the results of all 30 tests performed on F-65 sand against surfaces with Profiles 1 and 3, and all 36 tests performed on O20-30 sands against surfaces with Profiles 1, 2, and 3. Profile 1 mobilized peak and residual average frictional anisotropies between 7.2 and 3.8 kPa, Profile 2 mobilized average anisotropies between 5.0 and 3.8 kPa, and Profile 3 mobilized average anisotropies between 3.7 and 0.8 kPa.

The results indicate that surfaces with Profile 1 mobilized the largest amount of frictional anisotropy. Surfaces with Profile 3, which was inspired by the sidewinder snakes, mobilized the smallest amount of frictional anisotropy. This result may be related to the interactions between the scales and substrate during sidewinding locomotion. During sidewinding, alternate sections of the snake body are lifted from the substrate, moved forward, and placed in contact at a new location (Jayne 1986; Marvi et al. 2014; Astley et al. 2015). Sidewinding is then conceptually similar to legged

walking where the snake body sections that are lifted and advanced serve a function similar to feet during walking. As a result, it is likely that frictional anisotropy is not an essential trait of the sidewinding gait.

The results and discussion presented in the following sections are focused on tests performed with Profile 1, and Palumbo (2018) has provided a detailed description of the results from all tests against surfaces with Profiles 2 and 3.

Effect of Scale Geometrical Characteristics

A parametric study on the effect of scale height, H , and scale length, L , was undertaken to explore the independent effect of these parameters on the mobilized shear response. Increases in H while keeping L constant at 12 mm resulted in an increase in mobilized shear resistances and dilative volumetric changes, as shown in Figs. 7(a-d) for tests on F-65 sand in the cranial and caudal

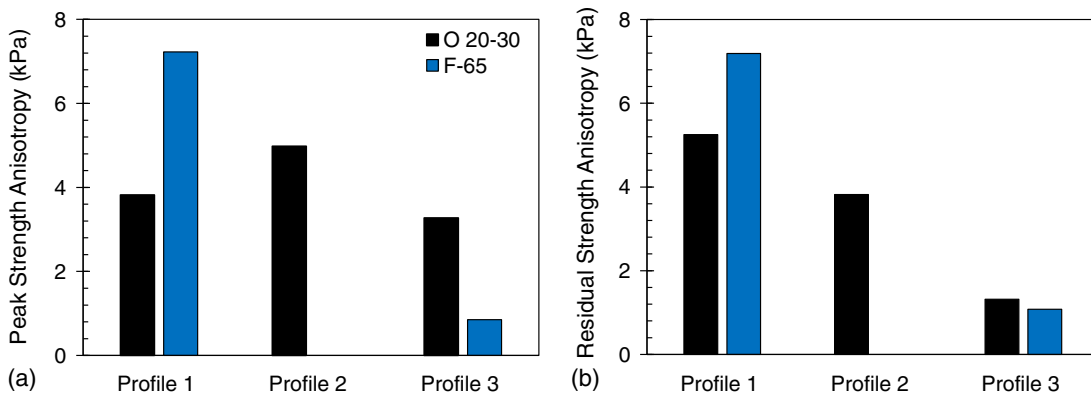


Fig. 6. (a) Peak; and (b) residual frictional anisotropy mobilized by bioinspired surfaces.

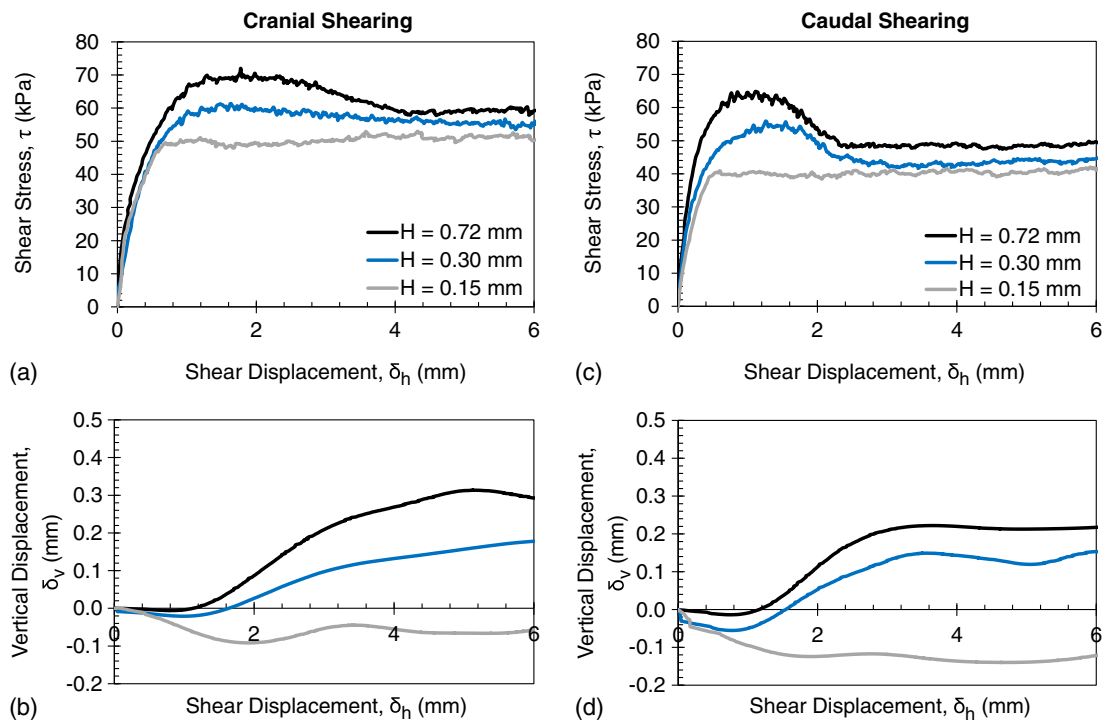


Fig. 7. Mobilized shear stresses and associated vertical displacements for interface shear tests on Ottawa F-65 sand against surfaces with varying scale height (Profile 1 with $L = 12$ mm) in (a and b) cranial; and (c and d) caudal directions.

directions. Tests against surfaces with H of 0.72 and 0.30 mm exhibited a dilative behavior, whereas tests against the surface with H of 0.15 mm exhibited contractive behavior. Figs. 8(a–f) present peak and residual stress ratios and dilation angles for tests on F-65 and O20-30 sands. Values from tests against the glued sand and untextured surfaces are also provided in the figures.

Increases in scale height resulted in increases in peak and residual stress ratio as well as in dilation angle for tests on both sands in both cranial and caudal directions. Initial increases in H from 0.10 to 0.30 mm resulted in a sharp increase in peak and residual stress ratios and dilation angles, whereas subsequent increases in H from 0.30 to 0.72 mm only resulted in modest increases. These trends agree with those presented by other authors where a limiting value of interface strength is reached as the surface roughness is increased (e.g., Uesugi and Kishida 1986; Subba Rao et al. 1998). The peak and residual stress ratio values from caudal tests with H smaller than or equal to 0.15 mm were close to those measured against the untextured surface.

Mobilized frictional anisotropy is evident for peak and residual stress ratios and dilation angles. Tests on F-65 sand yielded shear resistances in the cranial direction that are 17% and 19% larger for peak and residual conditions, respectively, compared with those mobilized in the caudal direction [Figs. 8(a–c)]. Similarly, tests on O20-30 yielded larger cranial values that are 12% and 28% larger for peak and residual, compared with caudal values [Figs. 8(d–f)].

Testing against surfaces with larger scale lengths while keeping the scale height constant at 0.30 mm mobilized smaller peak and residual shear resistances and smaller dilative vertical displacements, as shown in Figs. 9(a–d) for cranial and caudal tests on F-65 sand. For tests with the finer F-65 sand, initial increases in L from 6 to 18 mm resulted in a sharp decrease in mobilized peak and residual stress ratio, and further increases from 18 to 32 mm resulted in more moderate decreases in stress ratio [Figs. 10(a–c)].

The trends for tests with the coarser Ottawa 20-30 sand are somewhat different, with limited effect of L with initial increases from 6 to 12 mm, a sharp influence for L values between 12 and 24 mm, and limited influence for increases in L between 24 and 32 mm [Figs. 10(d–f)]. Generally, the surfaces with a low L (i.e., 6 mm) mobilized a shear behavior similar to that of a fully rough soil–structure interface, whereas surfaces with a large L (i.e., 32 mm) exhibited a behavior similar to that of a smooth interface. The frictional anisotropy decreased with increasing L for F-65 sand, but its magnitude remained relatively constant with L for tests on O 20-30. The sharp decrease in stress ratio occurs at L values between 6 and about 18 mm for tests with the finer F-65 sand, whereas this transitional behavior is observed at L values between 12 and 24 mm for tests with the coarser O 20-30 sand. This may suggest an effect of particle size, where the finer sand experiences this transition in behavior at distances equivalent to 30–90 D_{50} , and the coarser sand experiences the transition in behavior at distances roughly equivalent to 15–35 D_{50} .

PIV Analysis of Soil Deformations

PIV analyses were performed to further the understanding of shearing direction (i.e., cranial versus caudal) and scale geometry (i.e., scale height and scale length) on the induced soil deformations. Representative results from six tests are provided: (1) cranial and caudal tests against surfaces with $L = 24$ mm and $H = 0.30$; (2) cranial tests against surfaces of varying H (0.10 and 0.72 mm) and fixed length (12 mm); and (3) cranial tests against surfaces of varying L (12 and 32 mm) and fixed height (0.30 mm). The results presented here correspond to surface displacement increments of 3–5 mm, which capture the transition between peak and residual conditions. An analysis of the induced soil displacements during the entire test have been provided by Palumbo (2018).

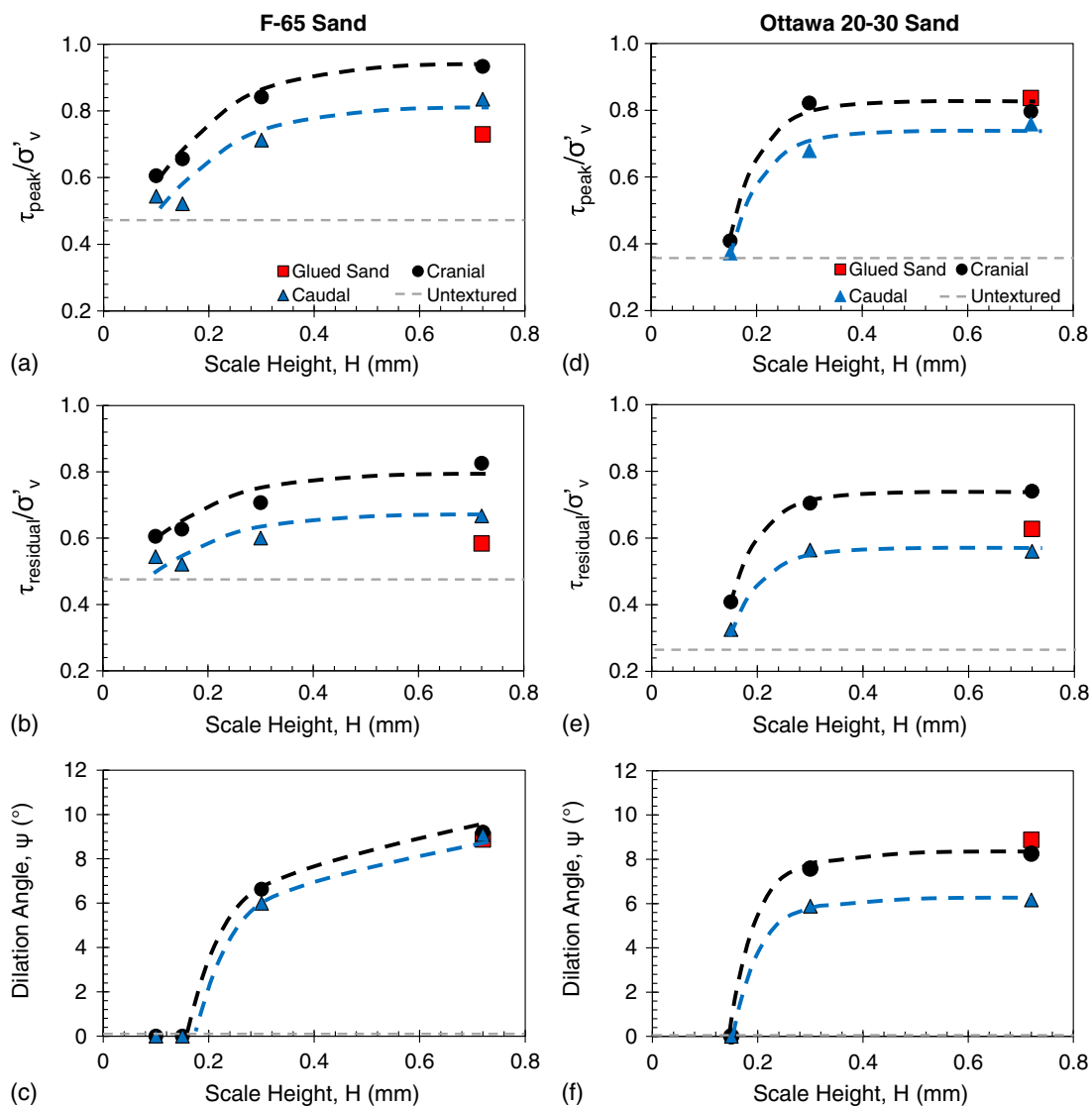


Fig. 8. Interface shear response as a function of scale height (Profile 1 with $L = 12$ mm) for tests on (a–c) F-65 sand; and (d–f) Ottawa 20-30 sand.

Shearing in the cranial direction developed wedges at the leading front of the scales where soil displacement, shear strains, and volumetric strains localized. On the other hand, caudal shearing induced deformations and strains that were more evenly distributed along the soil–structure interface. The resultant displacement, shear strain, and volumetric strain fields from PIV analyses during cranial and caudal tests are presented in Figs. 11(a–c), where negative values of volumetric strain indicate dilation. Cranial shearing led to soil dilation at the leading end of the scales and soil contraction at the trailing end. The soil within the wedges developed during cranial shearing is likely to experience local increases in mean effective stresses, indicative of passive conditions. The lack of well-defined wedges during caudal shearing suggests that the angle of the scale approaching the soil has an important effect on the development of local passive conditions (about 90° for cranial shearing and 1° for caudal), in general agreement with analogies used for development of classical stress-dilatancy theories (e.g., Rowe 1962).

The height of the asperities also influenced the trends in soil deformation during cranial tests, where surfaces with smaller H (0.10 mm) developed well-defined wedges, whereas surfaces with a larger H (0.72 mm) developed a shear band with more uniform

deformations, as shown in the displacement, shear strain, and volumetric strain fields presented in Figs. 12(a–c). The length of the asperities also had an important effect on the patterns in soil deformation during cranial tests, as shown in Figs. 13(a–c). The surface with the largest scale length (32 mm) developed a large passive wedge with dilation on the soil ahead of the scale and contraction on the soil behind the scale. On the other hand, the surface with the smaller length (12 mm) did not mobilize individual wedges, and the overall volumetric response was dilative. It is likely that the more uniform soil deformations observed in tests against surfaces with small L result from interaction of passive wedges ahead of the scales that developed a shear band. The magnitude of the average roughness parameter, R_a , is relatively insensitive to the value of L (Table 2), thus not being able to capture the different soil deformation mechanisms shown here.

Discussion and Implications for Geotechnical Engineering Practice

The results presented in the previous sections indicate that tests with snakeskin-inspired surfaces performed in the cranial direction

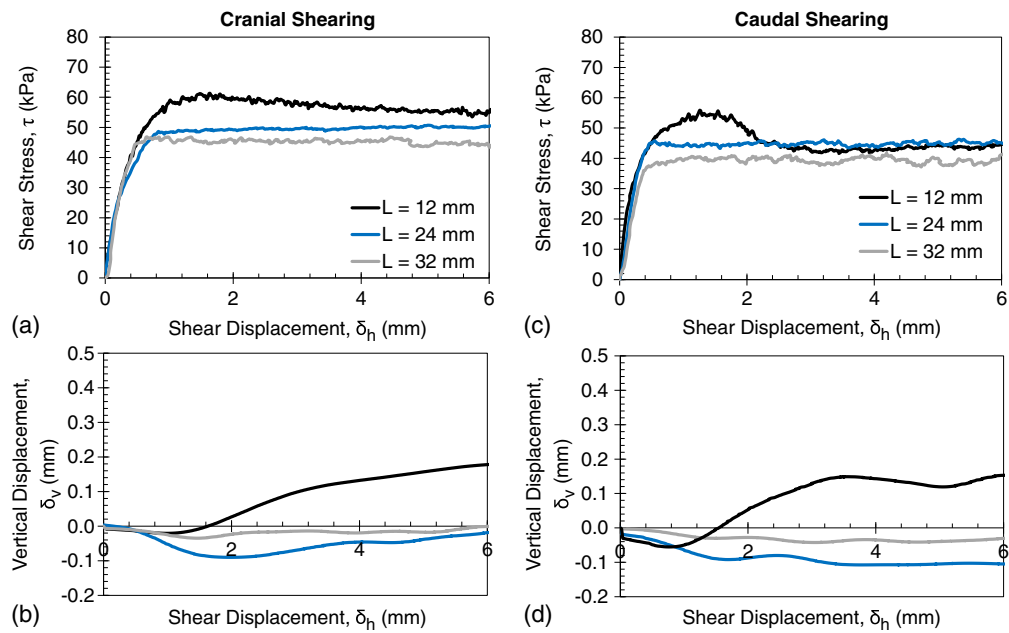


Fig. 9. Mobilized shear stresses and associated vertical displacements for interface shear tests on Ottawa F-65 sand against surfaces with varying scale length (Profile 1 with $H = 0.30$ mm) in (a and b) cranial; and (c and d) caudal directions.

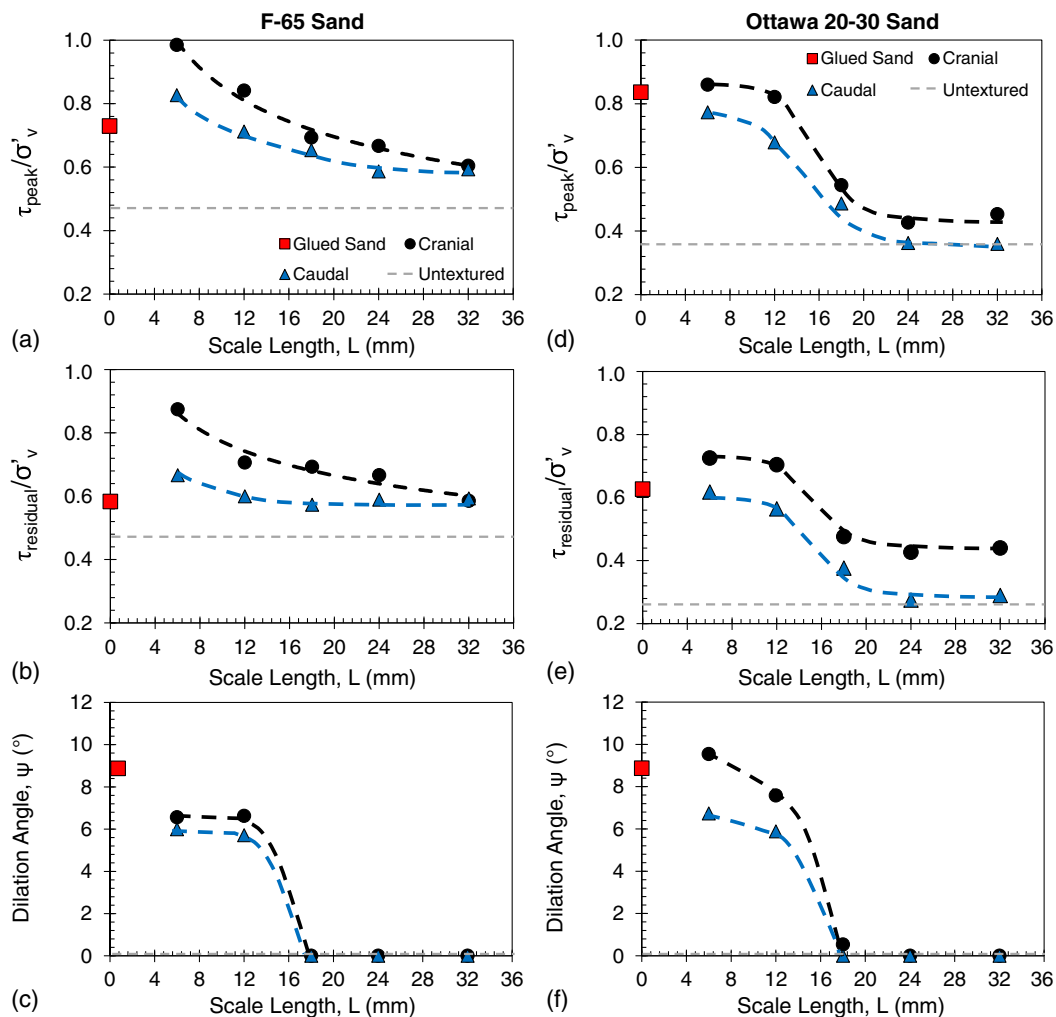


Fig. 10. Interface shear response as a function of scale length (Profile 1 with $H = 0.30$ mm) for tests on (a-c) F-65 sand; and (d-f) Ottawa 20-30 sand.

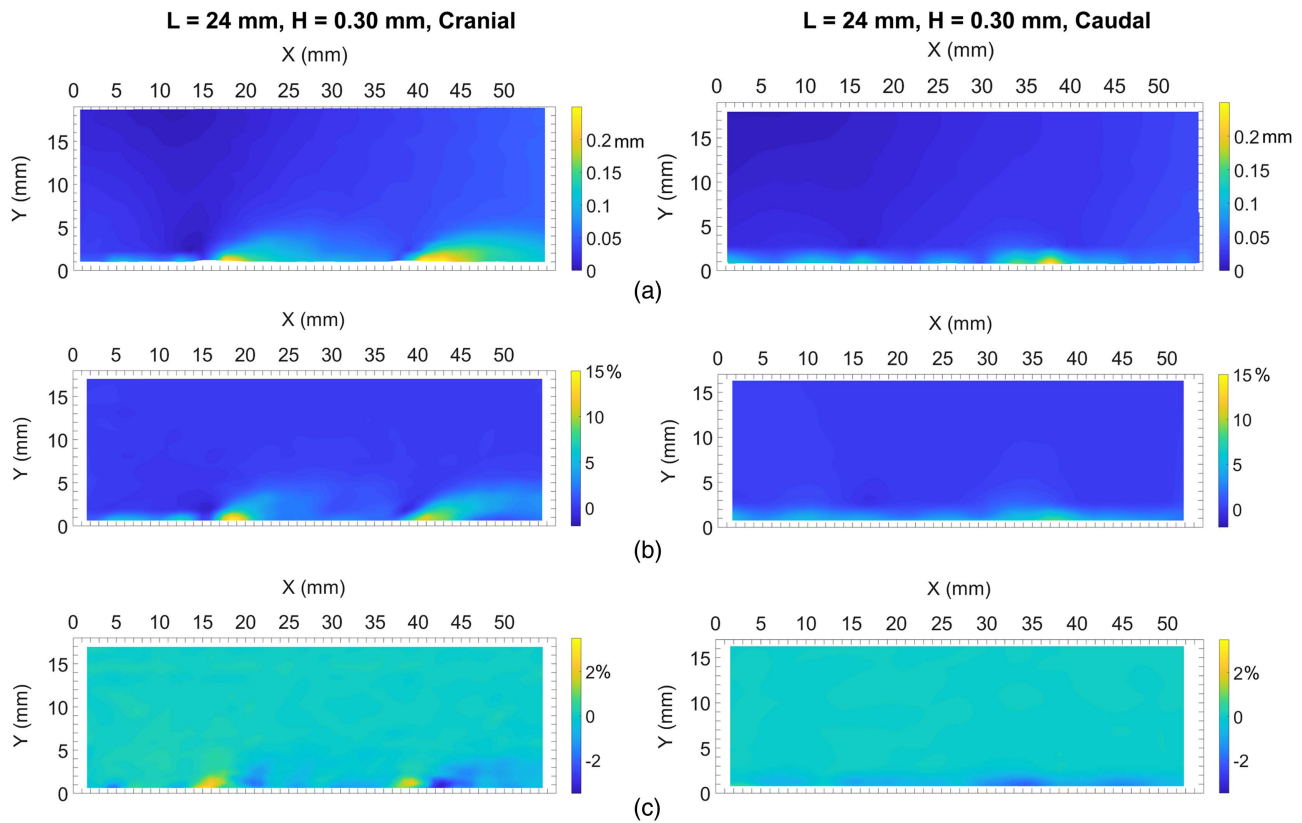


Fig. 11. PIV analysis on cranial and caudal tests against surfaces with scale length of 24 mm and scale height of 0.30 mm for 3–5-mm shear displacement increment: (a) resultant displacements; (b) shear strains; and (c) volumetric strains. The color scales vary, and negative volumetric strains indicate dilation.

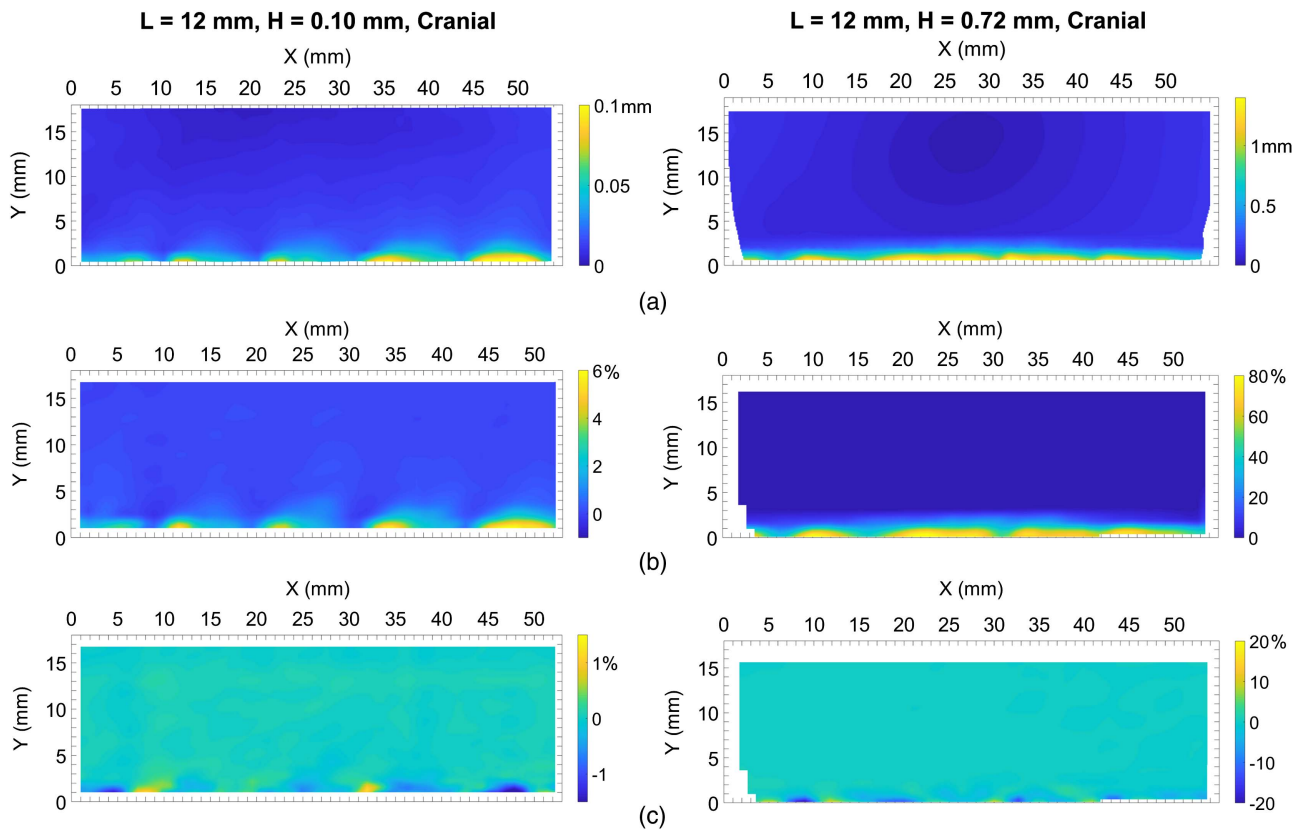


Fig. 12. PIV analysis on cranial tests against surfaces with scale height of 0.10 and 0.72 mm for 3–5-mm shear displacement increment: (a) resultant displacements; (b) shear strains; and (c) volumetric strains. Color scales vary, and negative volumetric strains indicate dilation.

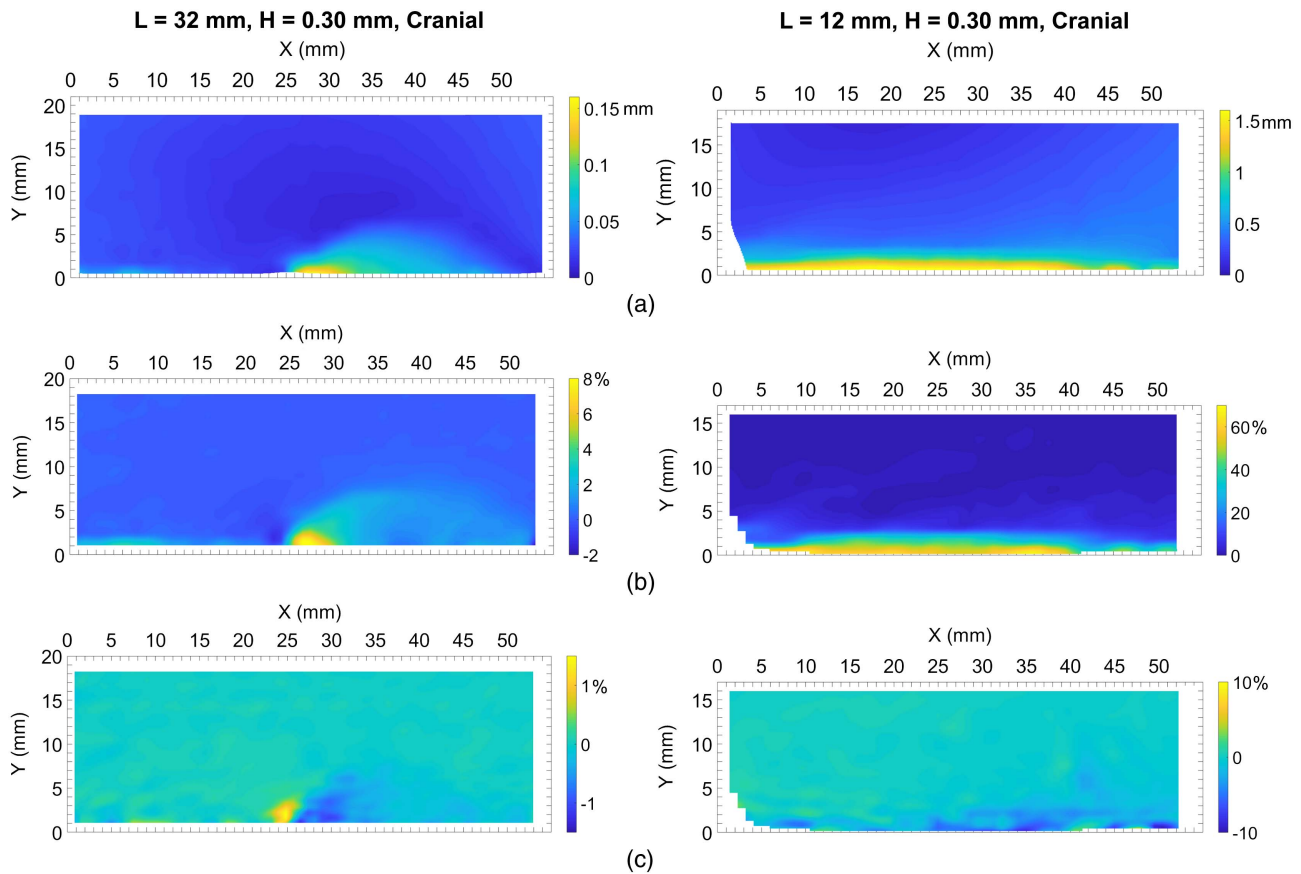


Fig. 13. PIV analysis on cranial tests against surfaces with scale length of 32 and 12 mm for 3–5-mm shear displacement increment: (a) resultant displacements; (b) shear strains; and (c) volumetric strains. Color scales vary, and negative volumetric strains indicate dilation.

mobilized larger shear resistances, dilation, and soil deformations than those performed in the caudal direction. The height and length of the bioinspired asperities also influenced the mobilized shear resistances and soil deformations. The scale geometry ratio, defined as the ratio of scale length to height (L/H), is introduced herein in an effort to capture the interface load-transfer mechanisms. The scales of surfaces with a large L/H value are more likely to mobilize individual soil deformation wedges, whereas the scales of surfaces with small L/H are more likely to develop shear bands with more uniform soil deformations characterized by dilation.

The results of all tests against bioinspired surfaces are plotted as a function of L/H in Figs. 14(a–c) for F-65 sand and Figs. 15(a–c) for O20-30 sand. The L/H ratio appears to unify the data from the tests against the bioinspired surfaces. Figs. 14(a and b) and 15(a and b) highlight the mobilized frictional anisotropy in terms of peak and residual stress ratios. Figs. 14(c) and 15(c) indicate that the dilation angle decreased as the L/H was increased, with larger dilation angles mobilized during cranial shearing than during caudal shearing. Figs. 14(d–f) and 15(d–f) provide the stress ratio and dilation angle results as a function of the average roughness. The trends with R_a exhibit large variability, especially at values between 0.07 and 0.10 mm, where the spread of the stress ratio and dilation angle data is as large as 0.5 and 8° , respectively. A comparison of trends obtained with the L/H and R_a parameters suggests that the former is better suited to capture interface load-transfer mechanisms, such as passive resistances, induced by surfaces with structured roughness form

composed of asperities that can independently modify the state of the soil locally around them. As shown by other authors (e.g., Uesugi and Kishida 1986; Dietz and Lings 2006; Martinez and Frost 2017), R_a is well-suited to describe the relationship with interface strength for surfaces with random form produced by processes such as abrasion.

Previous studies by Hryciw and Irsyam (1993) on the interface behavior between sands and ribbed surfaces with L/H of 13.2, 10.1, and 2.0 (L of 33, 25.2, and 5.1 mm) indicated that the mobilized passive resistances and overall capacity diminished as the distance between asperities decreased. The surfaces studied by the authors had smaller L than all of those tested in the study presented herein. Thus, their results may be used to hypothesize that the interface strength mobilized by snakeskin-inspired surfaces would decrease as L/H is further decreased.

Use of bioinspired surfaces that mobilize frictional anisotropy may be beneficial for the capacity and efficiency of geotechnical systems that are loaded in different directions during their lifetime, including installation and service life, such as driven piles, soil anchors, anchors for offshore structures, tunnels, and geosynthetics. The trends presented in this paper are not limited to the behavior of bioinspired surfaces; they are expected to be prevalent among other conventional surfaces such as ribbed soil reinforcements and certain types of textured geomembranes. Future research should address other aspects, such as cyclic interface strength and stiffness degradation and frictional anisotropy during monotonic and cyclic shearing on fine-grained soils.

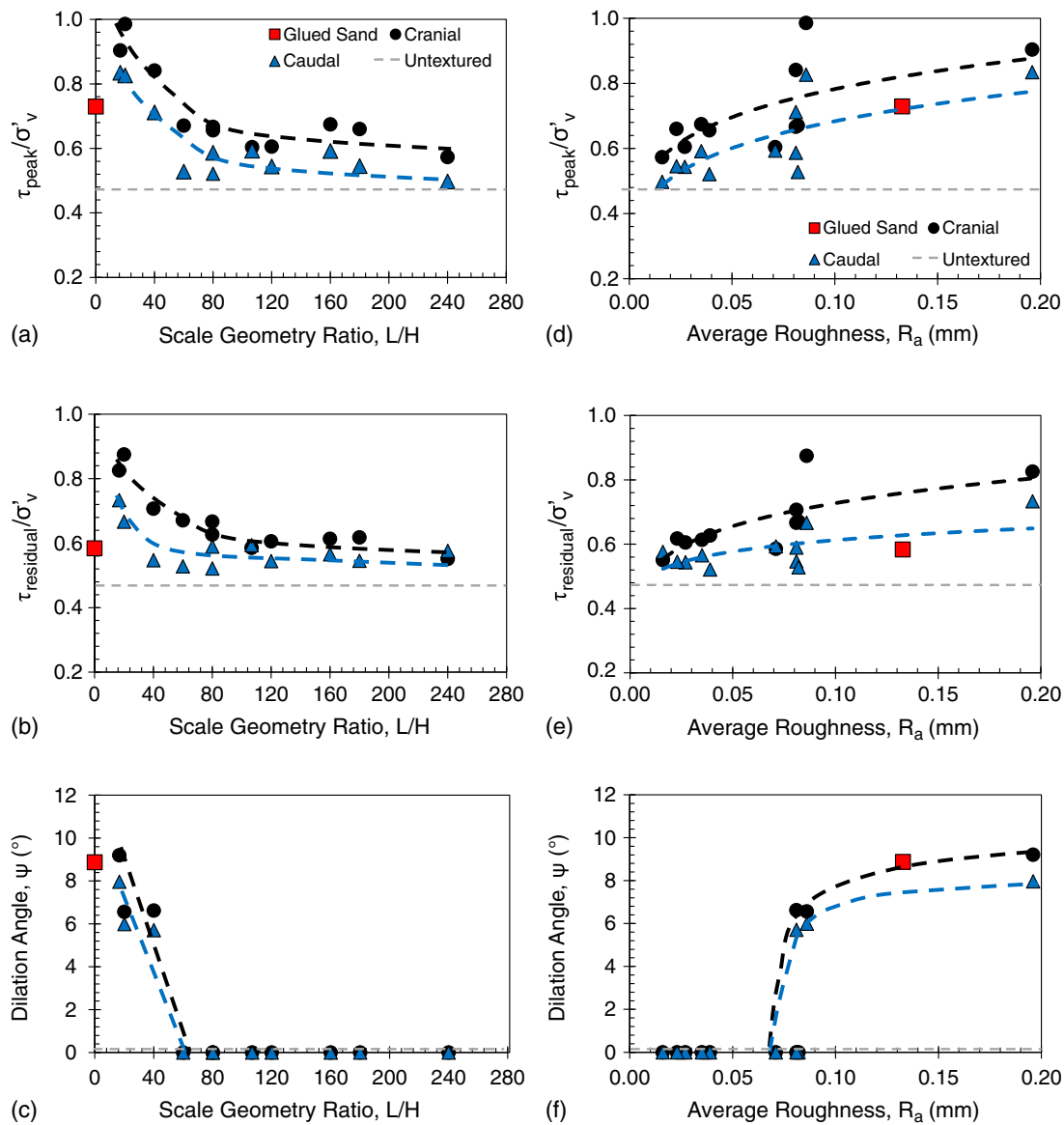


Fig. 14. Interface shear response for tests between Ottawa F-65 sand and surfaces with Profile 1 as a function of (a–c) scale geometry ratio; and (d–f) average surface roughness.

Conclusions

The experimental investigation presented herein consisted of monotonic interface shear box tests performed on specimens of subrounded sands of different particle sizes sheared against surfaces bioinspired by the ventral scales of three snake species. A subset of experiments analyzed using PIV revealed soil deformation mechanisms within the soil specimens. The results highlight the following trends:

- Shearing against the scales (i.e., cranial direction) consistently mobilized larger shear resistances and dilation angles than shearing along the scales (i.e., caudal direction). The shape of the scales (i.e., straight, concave, or convex) influenced the magnitude of the mobilized frictional anisotropy where shearing against straight and concave scales mobilized larger frictional anisotropy than against convex scales.
- The scale height, H , and length, L , of the snakeskin-inspired surfaces significantly influenced the shear behavior. Increases in H resulted in an increase in shear resistances and dilation

angle, whereas increases in L caused a decrease in mobilized shear resistances and dilation angle.

- PIV analyses revealed that cranial shearing induced larger displacements and shear and volumetric strains within the soil than caudal shearing. The geometry of the scales also influenced the induced deformations, where surfaces with large H or small L (i.e., small L/H) induced relatively uniform soil deformations within the shear band. On the other hand, surfaces with small H or large L (i.e., large L/H) induced deformations in wedge-like zones ahead and behind of the scales.
- A newly introduced parameter, the scale geometry ratio (L/H), was shown to successfully unify the mobilized shear resistance and dilation angle measurements and qualitatively capture the interface load-transfer mechanisms. Small L/H values describe surfaces more likely to induce large shear resistances, relatively uniform soil deformations, and an overall dilative response. On the other hand, large L/H values correspond to surfaces that mobilize smaller shear resistances along with soil deformations

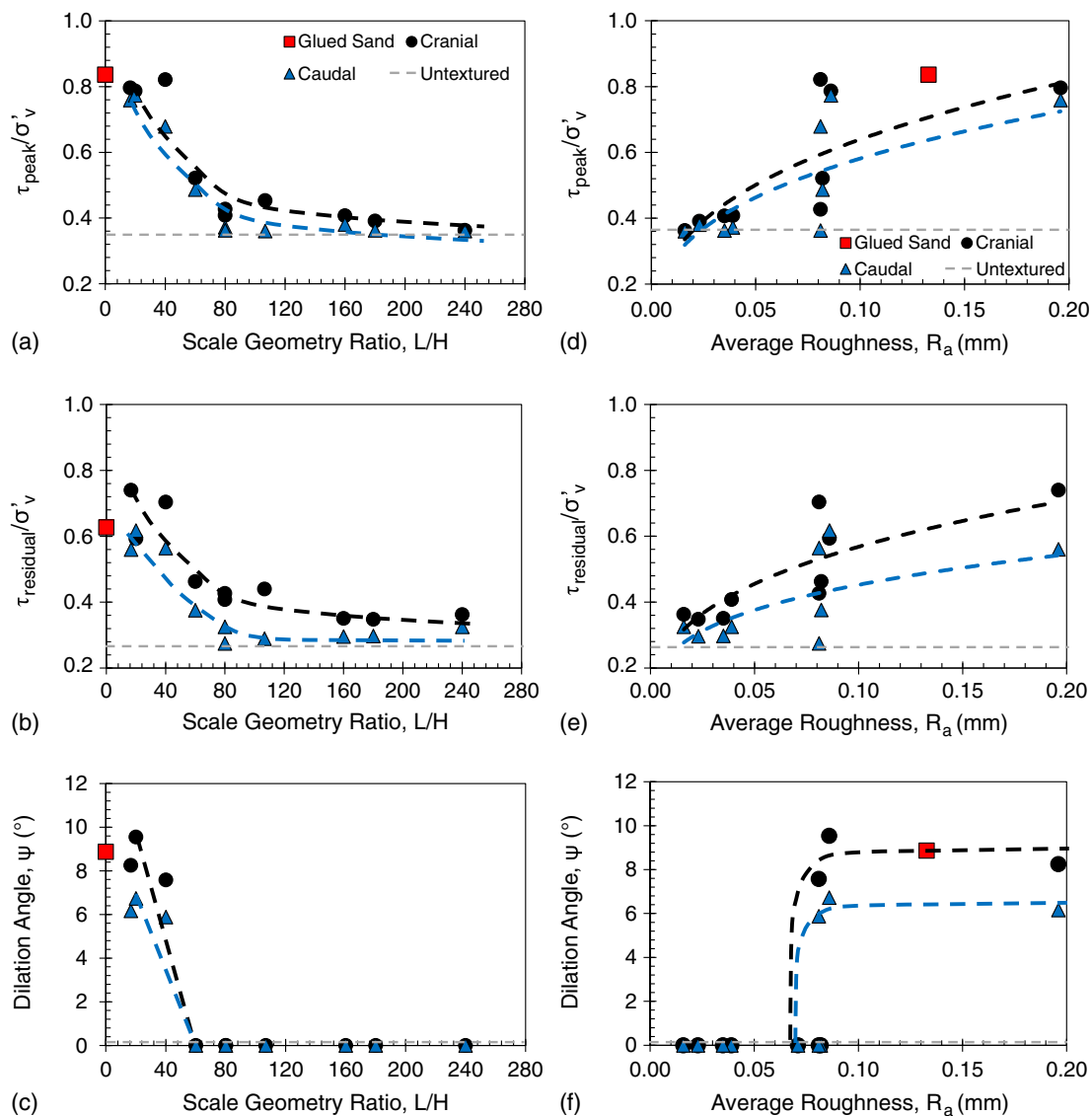


Fig. 15. Interface shear response for tests between Ottawa 20-30 sand and surfaces with Profile 1 as a function of (a–c) scale geometry ratio; and (d–f) average surface roughness.

in passive wedges ahead of the scales and an overall contractive behavior.

Acknowledgments

The studies presented in this paper are being undertaken by researchers in the NSF-funded ERC on Biomediated and Bioinspired Geotechnics (CBBG). The support of NSF through PTE Federal Award No. EEC-1449501 is acknowledged. The authors would like to thank the Museum of Vertebrate Zoology at the University of California, Berkeley, and Carol Spencer for the specimen loan.

References

- Astley, H. C., C. Gong, J. Dai, M. Travers, M. M. Serrano, P. A. Vela, H. Choset, J. R. Mendelson, D. L. Hu, and D. I. Goldman. 2015. "Modulation of orthogonal body waves enables high maneuverability in sidewinding locomotion." *Proc. Natl. Acad. Sci. USA* 112 (19): 6200–6205. <https://doi.org/10.1073/pnas.1418965112>.
- Benz, M. J., A. E. Kovalev, and S. N. Gorb. 2012. "Anisotropic frictional properties in snakes." *Proc. SPIE 8339 Bioinspiration, Biomimetics, and Bioreplication 2012*. <https://doi.org/10.1117/12.916972>.
- DeJong, J. T., M. Burrall, D. W. Wilson, and D. J. Frost. 2017. "A bio-inspired perspective for geotechnical engineering innovation." In *Proc., Geotechnical Frontiers 2017*, 862–870. Reston, VA: ASCE.
- DeJong, J. T., M. F. Randolph, and D. J. White. 2003. "Interface load transfer degradation during cyclic load: A microscale investigation." *Soils Found.* 43 (4): 81–93. https://doi.org/10.3208/sandf.43.4_81.
- DeJong, J. T., and Z. J. Westgate. 2009. "Role of initial state, material properties, and confinement condition on local and global soil-structure interface behavior." *J. Geotech. Geoenviron. Eng.* 135 (11): 1646–1660. [https://doi.org/10.1061/\(ASCE\)1090-0241\(2009\)135:11\(1646\)](https://doi.org/10.1061/(ASCE)1090-0241(2009)135:11(1646)).
- Dietz, M., and M. Lings. 2006. "Postpeak strength of interfaces in a stress-dilatancy framework." *J. Geotech. Geoenviron. Eng.* 132 (11): 1474–1484. [https://doi.org/10.1061/\(ASCE\)1090-0241\(2006\)132:11\(1474\)](https://doi.org/10.1061/(ASCE)1090-0241(2006)132:11(1474)).
- Dove, J. E., and D. J. Frost. 1999. "Peak friction behavior of smooth geomembrane-particle interfaces." *J. Geotech. Geoenviron. Eng.* 125 (7): 544–555. [https://doi.org/10.1061/\(ASCE\)1090-0241\(1999\)125:7\(544\)](https://doi.org/10.1061/(ASCE)1090-0241(1999)125:7(544)).
- Dove, J. E., and D. J. Jarrett. 2002. "Behavior of dilative sand interfaces in a geotribology framework." *J. Geotech. Geoenviron. Eng.* 128 (1): 25–37. [https://doi.org/10.1061/\(ASCE\)1090-0241\(2002\)128:1\(25\)](https://doi.org/10.1061/(ASCE)1090-0241(2002)128:1(25)).

- Durso, A. M. 2011. "Interactions of diet and behavior in a death-feigning snake (*Heterodon nasicus*)." M.S. thesis, Dept. of Biological Studies, Eastern Illinois Univ.
- Farhadi, B., and A. Lashkari. 2017. "Influence of soil inherent anisotropy on behavior of crushed sand-steel interfaces." *Soils Found.* 57 (1): 111–125. <https://doi.org/10.1016/j.sandf.2017.01.008>.
- Frost, J. D., A. Martinez, S. D. Mallett, and M. M. Roozbahani. 2017. "Intersection of modern soil mechanics with ants and roots." In *Proc., Geotechnical Frontiers 2017*, 900–909. Reston, VA: ASCE.
- Goel, A. K., S. Vattam, B. Wiltgen, and M. Helms. 2014. "Information-processing theories of biologically inspired design." In *Biologically inspired design*, edited by A. Goel, D. McAdams, and R. Stone. London: Springer. https://doi.org/10.1007/978-1-4471-5248-4_6.
- Gray, J., and H. W. Lissmann. 1950. "The kinetics of locomotion of the grass-snake." *J. Exp. Biol.* 26: 354–367.
- Hazel, J., M. Stone, M. S. Grace, and V. V. Tsukruk. 1999. "Nanoscale design of snake skin for reptation locomotion via friction anisotropy." *J. Biomech.* 32 (5): 477–484. [https://doi.org/10.1016/S0021-9290\(99\)00013-5](https://doi.org/10.1016/S0021-9290(99)00013-5).
- Helms, M., S. S. Vattam, and A. K. Goel. 2009. "Biologically inspired design: Process and products." *Des. Stud.* 30 (5): 606–622. <https://doi.org/10.1016/j.destud.2009.04.003>.
- Ho, T. Y. K., R. J. Jardine, and N. Anh-Minh. 2011. "Large-displacement interface shear between steel and granular media." *Geotechnique* 61 (3): 221–234. <https://doi.org/10.1680/geot.8.P.086>.
- Hryciw, R. D., and M. Irsyam. 1993. "Behavior of sand particles around rigid ribbed inclusions during shear." *Soils Found.* 33 (3): 1–13. https://doi.org/10.3208/sandf1972.33.3_1.
- Jayne, B. C. 1986. "Kinematics of terrestrial snake locomotion." *Copeia* 1986 (4): 915–927. <https://doi.org/10.2307/1445288>.
- Lillywhite, H. B. 2014. *How snakes work: Structure, function and behavior of the world's snakes*. New York: Oxford University Press.
- Mak, T. W., and L. H. Shu. 2004. "Abstraction of biological analogies for design." *Ann. CIRP* 53 (1): 117–120. [https://doi.org/10.1016/S0007-8506\(07\)60658-1](https://doi.org/10.1016/S0007-8506(07)60658-1).
- Martinez, A., and J. D. Frost. 2017. "The influence of surface roughness form on the strength of sand-structure interfaces." *Geotech. Lett.* 7 (1): 1–8. <https://doi.org/10.1680/jgele.16.00169>.
- Martinez, A., J. D. Frost, and G. L. Hebel. 2015. "Experimental study of shear zones formed at sand/steel interfaces in axial and torsional axisymmetric tests." *ASTM Geotech. Test. J.* 38 (4): 409–426. <https://doi.org/10.1520/GTJ20140266>.
- Martinez, A., and S. Palumbo. 2018. "Anisotropic shear behavior of structure interfaces: Bio-inspiration from snake skin." In *Proc., IFCEE 2018 Conf.*, 99–104. Reston, VA: ASCE.
- Martinez, A., and H. H. Stutz. 2019. "Rate effects on the interface shear behavior of normally and over-consolidated clay." *Geotechnique*. <https://doi.org/10.1680/jgeot.17.p.311>.
- Marvi, H. 2013. "The role of functional surfaces in the locomotion of snakes." Ph.D. dissertation, Dept. of Mechanical Engineering, Georgia Institute of Technology.
- Marvi, H., J. P. Cook, J. L. Streater, and D. L. Hu. 2016. "Snakes move their scales to increase friction." *Biotribology* 5 (3): 52–60. <https://doi.org/10.1016/j.biotri.2015.11.001>.
- Marvi, H., C. Gong, N. Gravish, H. Astley, M. Travers, R. L. Hatton, J. R. Mendelson III, H. Choset, D. L. Hu, and D. I. Goldman. 2014. "Sidewinding with minimal slip: Snake and robot ascent of sandy slopes." *Science* 346 (6206): 224–229. <https://doi.org/10.1126/science.1255718>.
- Marvi, H., and D. L. Hu. 2012. "Friction enhancement in concertina locomotion of snakes." *J. R. Soc.* 9 (76): 3067–3080. <https://doi.org/10.1098/rsif.2012.0132>.
- Palumbo, S. 2018. "Anisotropic interface shear behavior of granular soil and surfaces biologically-inspired by snakeskin." M.S. thesis, Dept. of Civil and Environmental Engineering, Univ. of California, Davis.
- Rowe, P. W. 1962. "The stress-dilatancy relationship for static equilibrium of an assembly of particles in contact." *Proc. R. Soc. London, Ser. A* 269 (1339): 500–527. <https://doi.org/10.1098/rspa.1962.0193>.
- Stanier, S., J. Blaber, W. Take, and D. J. White. 2016. "Improved image-based deformation measurement for geotechnical applications." *Can. Geotech. J.* 53 (5): 727–739. <https://doi.org/10.1139/cgj-2015-0253>.
- Subba Rao, K. S., M. M. Allam, and R. G. Robinson. 1998. "Interfacial friction between sands and solid surfaces." *Proc. Inst. Civ. Eng. Geotech. Eng.* 131 (2): 75–82. <https://doi.org/10.1680/igeng.1998.30112>.
- Uesugi, M., and H. Kishida. 1986. "Influential factors of friction between steel and dry sands." *Soils Found.* 26 (2): 33–46. https://doi.org/10.3208/sandf1972.26.2_33.
- Uesugi, M., H. Kishida, and Y. Tsubakihara. 1989. "Friction between sand and steel under repeated loading." *Soils Found.* 29 (3): 127–137. https://doi.org/10.3208/sandf1972.29.3_127.
- Vangla, P., and G. M. Latha. 2015. "Influence of particle size on the friction and interfacial shear strength of sands with similar morphology." *Int. J. Geosynth. Ground Eng.* 1 (6): 1–12. <https://doi.org/10.1007/s40891-014-0008-9>.
- White, D. J., W. A. Take, and M. D. Bolton. 2001. "Measuring soil deformation in geotechnical models using digital images and PIV analysis." In *Proc., 10th Int. Conf. on Computer Methods and Advances in Geomechanics*, 997–1002. Boca Raton, FL: CRC Press.
- Zhou, B. L. 2000. "Bio-inspired study of structural materials." *Mat. Sci. Eng. C* 11 (1): 13–18. [https://doi.org/10.1016/S0928-4931\(00\)00136-3](https://doi.org/10.1016/S0928-4931(00)00136-3).